MATERIALS SCIENCE

Distributed direct air capture by carbon nanofiber air filters

Ronghui Wu[1,2], Hernan E. Delgado[3], Yi Xie[4], Yuanke Chen[1], Gangbin Yan[1], Edward Luo[1], Qizhang Li[1], Qingsong Fan[1], Yu Han[1], Genesis M. Higueros[1,4], Amar Ruthen[5], Chenxi Sui[1], Adarsh Suresh[1], David B. Mitzi[4,5], Chong Liu[1], Amgad Elgowainy[3], Po-Chun Hsu[1]*

The rising atmospheric CO_2 concentration is one of the biggest challenges human civilization faces. Direct air capture (DAC) that removes CO_2 from the atmosphere provides great potential in carbon neutralization. However, the massive land use and capital investment of centralized DAC plants and the energy-intensive process of adsorbent regeneration limit its wide employment. We develop a distributed carbon nanofiber (CNF)–based DAC air filter capable of adsorbing CO_2 downstream in ventilation systems. The DAC air filter not only has the potential to remove 596 $MtCO_2$ $year^{-1}$ globally but can also decrease energy consumption in existing building systems. The CNF-based adsorbent has a capacity of 4 mmol/g and can be regenerated via solar thermal or electrothermal methods with low carbon footprints. Through life cycle assessment, the CNF air filter shows a carbon removal efficiency of 92.1% from cradle to grave. Additionally, techno-economic analysis estimates a cost of $209 to 668 in capturing and storing 1 tonne of CO_2 from direct air.

INTRODUCTION

The increasing atmospheric greenhouse gas concentration that leads to intensifying global warming has become a critical environmental concern (*1*). The atmospheric CO_2 concentration, which was 280 parts per million (ppm) in the preindustrial period, has increased rapidly to exceed 420 ppm in 2021 (*2*), caused by human activities that release around 36 billion tonnes (Gt) of CO_2 annually (*3*). Carbon capture and storage (CCS) technology is crucial for achieving carbon neutrality, thereby effectively combating climate change (*4*). To realize net zero emission at the end of the century, direct air capture (DAC), a negative emission technology that can directly remove CO_2 from the atmosphere (*5*, *6*), will play a crucial role by removing ~10 Gt/year of CO_2 globally by mid-century, and ~20 Gt/year of CO_2 by the late 2090s (*7*). Compared with carbon capture from substantial point sources with high CO_2 concentration, such as fossil-fuel power stations and steel, cement, and chemical plants, DAC aims to tackle the 420 ppm of CO_2 and reverse the anthropogenic emissions back to normal. In theory, the CO_2 in the atmosphere is uniform enough for DAC to work anywhere without location restriction; however, the extensive land use and capital expenditure of DAC plants and the energy-intensive process of adsorbent regeneration limits its wide employment (*8*). Inferring from the historical development from centralized solar farms to distributed rooftop solar panels, it is anticipated DAC should become distributed to fully use its potential to accelerate our efforts in combating global warming.

Same as rooftops provide existing access to solar energy without additional land use, buildings can also support DAC through the existing ventilation systems. In industrialized countries, people spend ~90% of their time indoors, such as homes, schools, and offices (*9*, *10*). Ample ventilation is necessary to ensure indoor air quality and occupant comfort (*9*, *11*). Integrating and retrofitting DAC units to the air filters in building indoor ventilation systems holds great CO_2 capture potential due to its widespread distribution and abundant resources (Fig. 1, A and B, and text S1). In addition, it can reduce the energy consumption for heating, ventilation, and air-conditioning (HVAC) by decreasing outdoor ventilation requirements (Fig. 1C), which accounts for 30% of global energy consumption and emits 10% of greenhouse gases globally (*12*, *13*).

Now, many materials have been developed for DAC, i.e., aqueous amine solutions (*14*, *15*), redox-active adsorbents using electrochemical methods (*16*–*20*), calcium sodium hydroxide adsorbent (*21*–*23*), amine-functionalized solid adsorbents (*24*–*28*), and metal-organic framework materials (*29*, *30*), etc. While holding excellent properties in eliminating CO_2 from the air, these techniques are not conformal to retrofitting air filtration. The liquid-phase absorbent requires an additional pumping and dispensing system that is complicated to be integrate into individual buildings. Other solid adsorbents are usually in powder form, which can cause substantial air pressure drop. More critically, current DAC adsorbents require high energy for regeneration. For example, it requires 225 to 357 kJ/mol CO_2 of thermal energy to regenerate calcium sodium hydroxide adsorbent (*31*), 172 kJ/mol CO_2 for aqueous monoethanolamine (MEA) solution (*32*), and 92 to 317 kJ/mol CO_2 for amine-functionalized solid adsorbents (*16*, *33*). Although the regeneration energy is anticipated to be high, considering the strong thermodynamic driving force required to capture CO_2 at the atmospheric concentration, the state-of-the-art regeneration energies are still considerably higher than the thermodynamic limits. The inefficiencies are mainly attributed to the low mass loading ratio of the active sorbents to the inactive substrates and the loss through waste heat that is too low-grade to recover. To realize distributed DAC, it is necessary to develop a solid adsorbent that is not only compatible with air filter systems with low-pressure drop and low-energy consumption but also can be regenerated in a green and economical manner.

[1]Pritzker School of Molecular Engineering, University of Chicago, Chicago, IL 60637, USA. [2]School of Materials Science and Engineering, Nanyang Technological University, 50 Nanyang Avenue, Singapore, Singapore. [3]Argonne National Laboratory, Lemont, IL 60439, USA. [4]Thomas Lord Department of Mechanical Engineering and Materials Science, Duke University, Durham, NC 27708, USA. [5]Department of Chemistry, Duke University, Durham, NC 27708, USA.
*Corresponding author. Email: pochunhsu@uchicago.edu

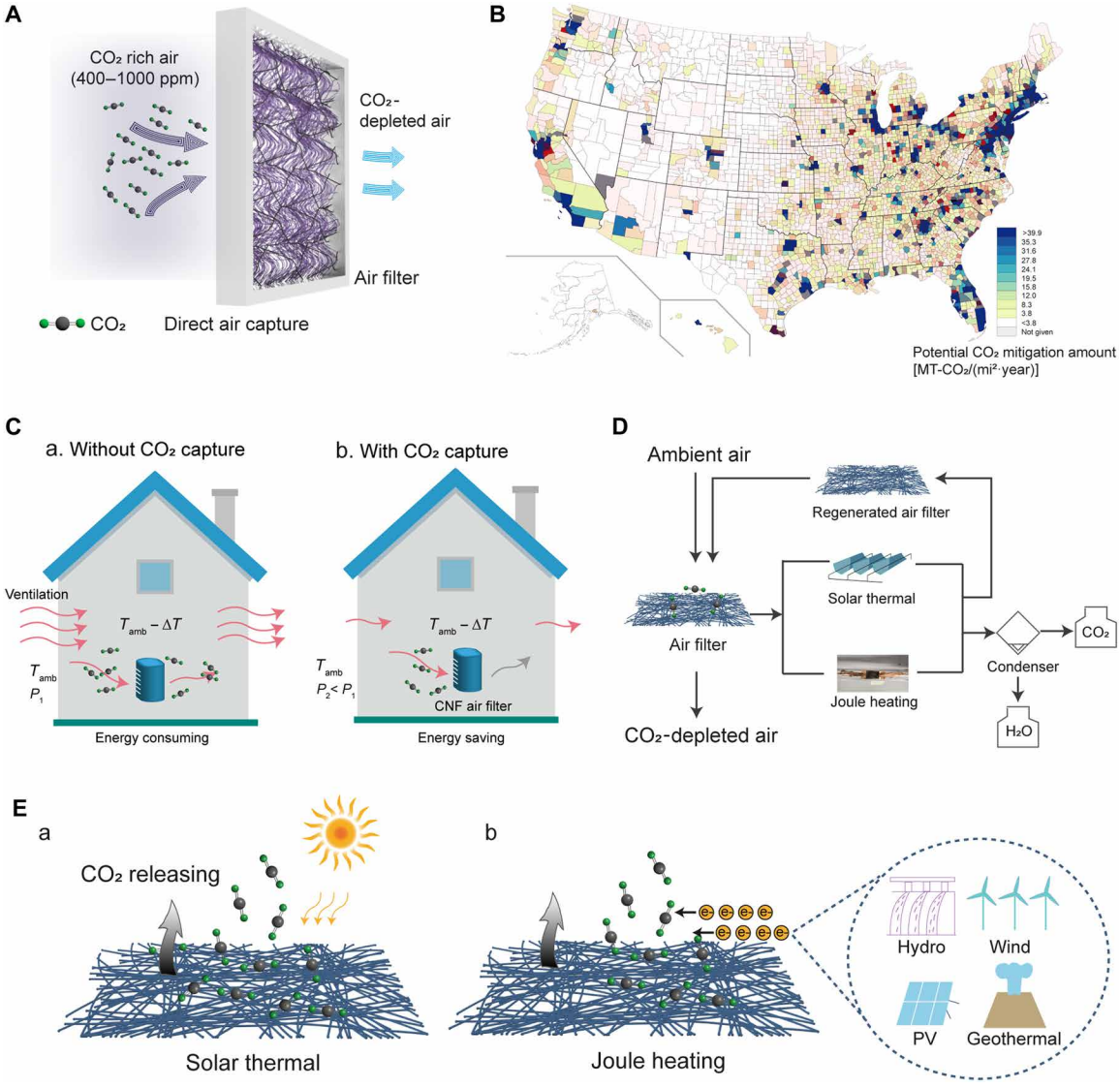

Fig. 1. Concept and advantages of DAC air filter using CNF-based adsorbents. (**A**) Schematic showing the air filter adsorbing CO_2 from the passing air. (**B**) The US map of the potential annual CO_2 mitigation amount by DAC air filters. (**C**) Energy saving scheme in the HVAC system: (a) without a DAC air filter, more outdoor ventilation is required to maintain indoor CO_2 concentration at a safe and healthy level for the occupants, while (b) with a DAC air filter, less ventilation is needed. (**D**) Flowchart of the CNF-based carbon capture air filter system, which consists of cyclic adsorption and desorption processes operated by renewable electricity or direct solar heating. (**E**) Schematic showing CNF-based adsorbents regenerated by (a) solar thermal or (b) Joule heating powered by renewable energy sources. PV, photovoltaic.

Here, we develop a carbon nanofiber (CNF)–based polyethylenimine (PEI) DAC air filter that can adsorb CO_2 within the ventilation system in buildings, which not only has high DAC capacity but can reduce HVAC energy consumption. The large surface area and porous structure of the CNF enable a high PEI mass loading while maintaining fast adsorption and desorption kinetics, leading to a remarkable carbon capture capacity. CNF has excellent solar absorptivity, electrical conductivity, and low heat capacity, enabling the adsorbent to be regenerated by solar thermal and/or electrothermal methods, both with renewable energy sources (Fig. 1, D and E). The total carbon footprint and environmental impacts of the whole CCS process for the air filter system are evaluated using life-cycle assessment (LCA), showing an overall cradle-to-grave CCS efficiency of 92.1% using solar thermal regeneration.

RESULTS

Fabrication, adsorption capacity, and kinetics of CNF-based adsorbent for DAC

The DAC air filter is fabricated by impregnating branched PEI on CNF nonwoven framework, which is obtained by electrospinning and pyrolysis of polyacrylonitrile (PAN). Briefly, PAN nanofibers were fabricated using a electrospinning technique, followed by oxidation at 260°C in air to stabilize the structure, and pyrolysis at 900°C in argon to obtain the CNF with high carbon yield (56%) and high electrical conductivity due to graphitization. Afterward, a thin layer of branched PEI with controllable mass loading was impregnated on CNF nonwoven framework to get the CNF-based adsorbent (Fig. 2A). The PAN nanofibers have round cross section with an average diameter of 230 nm, which further shrinks to around 197 nm

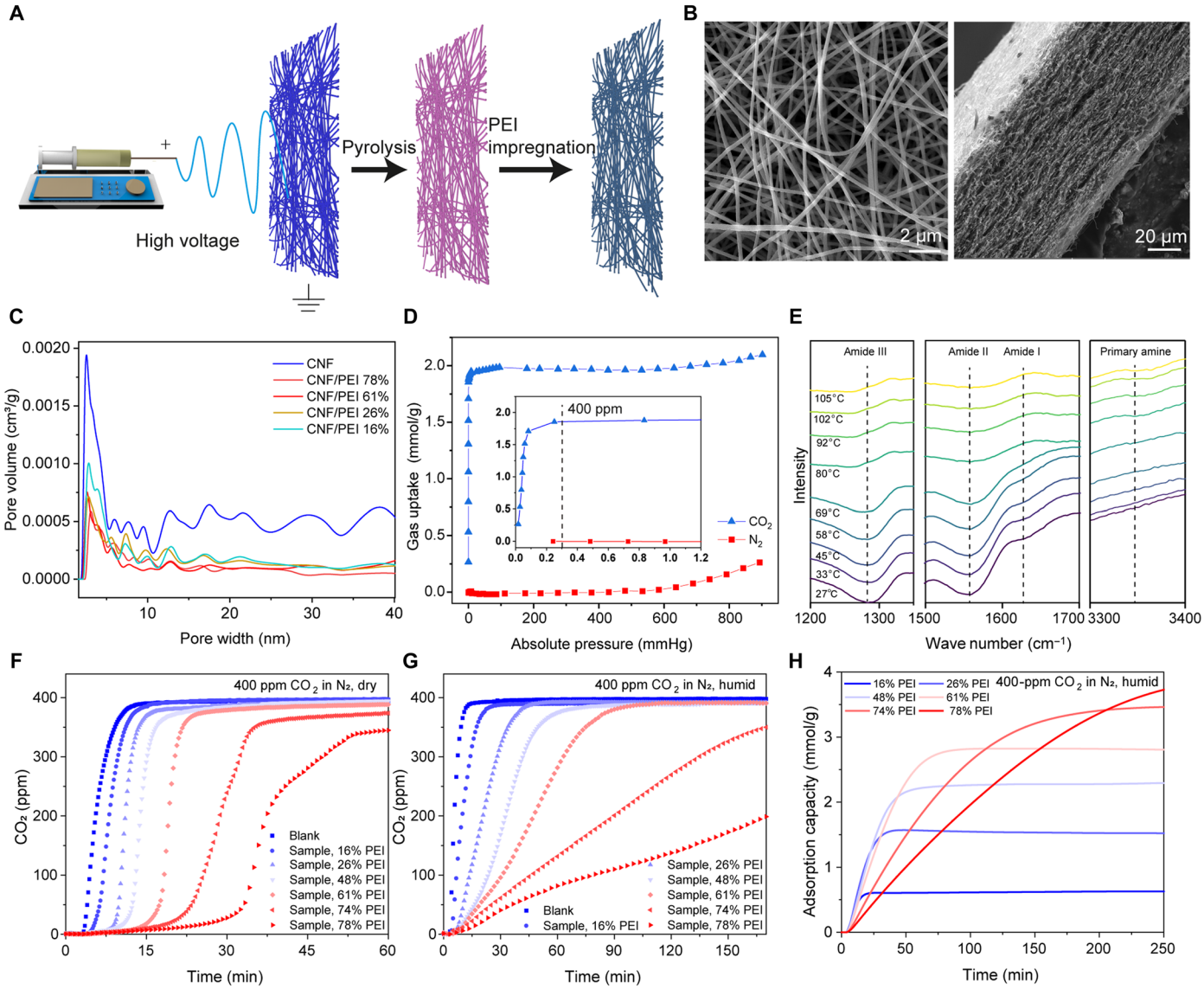

Fig. 2. Fabrication and CO_2 adsorption capability of the DAC air filter. (**A**) Preparation of the DAC air filter, including electrospinning, pyrolysis, and PEI impregnation. (**B**) SEM images showing the surface and cross-sectional morphology of CNF nonwoven. (**C**) Pore distribution curves of CNFs before and after PEI impregnation. (**D**) CO_2 and N_2 adsorption isotherms of DAC air filter at 25°C. Inset is the enlarged figure showing the high CO_2 adsorption capacity and selectivity at 400 ppm of partial pressure. (**E**) In situ FTIR-ATR spectra of DAC air filter as the temperature increases from 27° to 105°C. (**F** to **G**) Breakthrough curves of DAC air filter with different PEI mass loading under (F) dry and (G) humid conditions. (**H**) Adsorption capacities of the DAC air filter measured with humid N_2 gas containing 400 ppm of CO_2.

after pyrolysis into CNF, as shown in SEM images in Fig. 2B and transmission electron microscopy (TEM) images in fig. S1. Raman spectrum shows clear D band and G band at 1348 and 1579 cm^{-1}, which corresponds to the defects and disorders, and the characteristic peak of sp^2-hybridized carbon structures, respectively (fig. S1C). The diffraction peaks at 43° (110) and 26° (002) also confirm the presence of ordered graphitic and amorphous carbon (fig. S1D) in the x-ray diffraction (XRD) spectrum (*34*).

Based on the N_2 adsorption isotherms, CNF has a surface area of 50.2 m^2/g with a mesoporous structure (fig. S2). It allows PEI to penetrate and distribute uniformly on the surface of the nonwoven. To decrease the solution viscosity and facilitate the mass flow, PEI is first diluted in methanol with various concentrations [1 to 20 weight % (wt %)] before impregnation, which results in different PEI mass loading of 16 to 78 wt % on CNF (PEI mass ratio in total adsorbent). As shown in the scanning electron microscopy (SEM) images (fig. S3) and energy-dispersive x-ray spectroscopy (EDS) results in fig. S4, PEI is coated uniformly on the CNF nonwoven surface, with N contents increased from 2.3 to 12.2%. In addition, the analysis of C, N, and O elements at five different spots along the thickness direction further demonstrates the uniform surface impregnation (fig. S4). PEI is firstly coated on a single fiber surface and then partially clusters and forms a thin membrane on the fiber network, blocking parts of interfibrous pores on the nonwoven (fig. S3). After impregnation with 61% PEI mass loading, the adsorbent still maintains a surface area value of 18.9 m^2/g (Fig. 2C).

The abundant amine groups on PEI-CNF adsorbent spontaneously react with CO_2 at low partial pressure (400 ppm), as shown in the CO_2 adsorption isotherms at 25°C (Fig. 2D). At CO_2 atmospheric partial pressure of 0.3 mmHg, the CO_2 adsorption capacity reaches to ~2 mmol/g, while that for N_2 remains negligibly low, demonstrating its excellent selectivity for CO_2 adsorption in air. The N_2 adsorption increases when the partial pressure is enhanced to 600 mmHg, attributed to the physisorption of porous CNF. Under dry conditions, primary or secondary amines react with CO_2 to form ammonium carbamate, which may further form into carbamic acid and bicarbonate with the assistance of water molecules under humid conditions (*35*, *36*). This enables the adsorbent to have a higher capacity in the humid atmosphere. The tertiary amine on the backbone of PEI can only react with CO_2 under humid conditions, forming bicarbonate (*35*). The detailed reaction mechanisms are shown in fig. S5. In situ Fourier transform infrared (FTIR)–attenuated total reflectance (ATR) spectra were taken to study the CO_2 adsorption and desorption mechanism, as shown in Fig. 2E. The adsorbent was saturated with CO_2 in the ambient atmosphere [22° to 28°C, 30 to 50% relative humidity (RH)]. At the temperature of 27°C, peaks at 1286, 1558, and 1633 cm^{-1} can be assigned to the C-N, COO-, and C═O stretching in carbamate or carbamic acid, respectively (*37*, *38*). After being heated to 80°C, these peaks diminish because of the endothermic desorption of CO_2 (*39*). Meanwhile, peaks at 3347 cm^{-1} that refer to the N-H stretching in primary amines intensify, demonstrating the reformation of amine groups on the carbon surface.

X-ray photoelectron spectroscopy (XPS) was used to characterize the surface properties of the as-synthesized CNF and the CNF/PEI adsorbent (fig. S6). Both samples exhibit the presence of carbon (C), nitrogen (N), and oxygen (O). The high-resolution N 1s spectrum of the pristine CNF shows two main peaks corresponding to pyridinic nitrogen (398.2 eV) and graphitic nitrogen (401.1 eV), which are attributed to the pyrolysis of oxidized PAN (*40*) (fig. S6B). After PEI impregnation, nitrogen from the amine functional groups dominates the N 1s spectrum. The peak that appears at 400.2 eV corresponds to the typical amine functional group (*41*), while the other peak at 401.5 eV (fig. S6C) can be assigned to the protonated nitrogen, associated with the formation of the carbamate ion (*41*), which forms when the adsorbent reacts with the CO_2 in the air.

Breakthrough tests were conducted to quantify the transient adsorption and investigate the kinetics of CNF adsorbents by purging CO_2/N_2 mixture gas (400 ppm of CO_2 in N_2, for simulating direct air) through the adsorbents and measuring downstream CO_2 concentrations in real time (fig. S7 and experimental section). Figure 2F shows the breakthrough curves of the CNF adsorbents with different PEI loadings under dry CO_2/N_2 mixture gas. With PEI mass loading increasing from 16 to 78%, it takes longer to be fully saturated with CO_2, indicating higher adsorption capacity. Under a humid atmosphere, the saturation time is further enhanced (Fig. 2G). By converting the breakthrough data into CO_2 adsorption capacity (Fig. 2H and fig. S8), CNF adsorbents show highest adsorption capacity of 4 mmol/g at humid conditions (68% RH) and 1.5 mmol/g at dry condition when PEI mass loading is 78%. Both the adsorption capacity and adsorption rate are enhanced under humid conditions compared to a dry environment because water works as a nucleophile and assists the CO_2-amine reaction (*36*). Under three different humid conditions, i.e., 0, 30, and 68% RH, the adsorption capacities are 1.1, 2.5, and 3.0 mmol/g, respectively, when PEI loading is 61 wt %, as shown in fig. S9. Meanwhile, the presence of water leads to a slower reaction rate, which can be attributed to the higher activation energy of the water-assisted pathway, making it kinetically less favored compared to the direct amine-CO_2 reaction mechanism (*36*). With PEI mass loading increasing to 78 wt %, the adsorption capacity has been enhanced owing to more amine groups on the CNF surface, but the thick coating of PEI also blocks the inter- and intraporous structures of CNF nonwoven (fig. S3) and therefore limits the CO_2 diffusion in the adsorbent, resulting in slower adsorption rate. At room temperature, the adsorption time at half capacity markedly increases when the PEI mass loading is enhanced to 74 and 78 wt % at both humid and dry conditions (fig. S5B), which is caused by the increasing PEI clogging on the CNF networks (fig. S1). When the PEI mass loading is 61 wt %, the adsorbent shows a high capacity of 3 mmol/g with a short adsorption time at half capacity of 27 min.

The effect of temperature on the adsorption capacity and amine efficiency is further explored. The amine efficiency (mol CO_2/mol N) refers to the molar ratio of captured CO_2 to the number of amine groups (*26*). With the temperature increasing from 25° to 80°C, the adsorption capacity and amine efficiency are both enhanced, due to the fast CO_2 diffusion, accelerated reaction kinetics, and improved polymer chain mobility under a high PEI loading of 78 wt % (fig. S10).

Desorption of CNF adsorbent using renewable energy

CNF adsorbent can be regenerated efficiently using either solar thermal or electrothermal approaches due to its intrinsic high solar absorptivity, decent electrical conductivity, low heat capacity, and low desorption temperature of amine-CO_2. Solar thermal regeneration holds great potential since it allows the direct conversion from solar radiation to the thermal energy of the adsorbents, without requirements for additional materials or energy resources. Compared to the current thermal regeneration methods using a boiler or furnace with enormous energy input (*42*), the solar thermal systems could minimize the carbon footprint. Figure 3A shows the solar absorptivity of CNF pyrolyzed at different temperatures from 600° to 900°C. When the pyrolyzing temperature is 900°C, the weight-averaged solar absorptivity (in reference to AM1.5) reaches up to 94.4%. We theoretically calculated the adsorbent temperature under different solar intensities (text S2). The adsorbent treated under 900°C can be heated up to the regeneration temperature (~80°C) when the solar intensity is 860 W/m^2 as shown in Fig. 3B. This enables the CO_2 to be desorbed from the CNF adsorbent under direct sunlight. To experimentally demonstrate this process, a solar simulator was used to generate solar power for the CNF adsorbent placed on a foam in an air-sealed quartz tube (fig. S11). The regenerated CO_2 was detected by the downstream sensor. Figure 3C shows the real-time regenerated CO_2 concentration under different solar intensities from 982 to 1882 W/m^2. Adsorbents were saturated at room atmosphere of 22 to 28°C and 30 to 50% RH before measurements. The desorption is accelerated under intensified solar intensity owing to the corresponding higher CNF temperatures. Ultimately, CO_2 can be removed from the adsorbents even at a solar intensity of 982 W/m^2 (fig. S12). The desorbed CO_2 from the CNF adsorbents with various PEI mass loading using solar thermal methods are shown in fig. S13. The desorption CO_2 capacity is more pronounced with the PEI mass

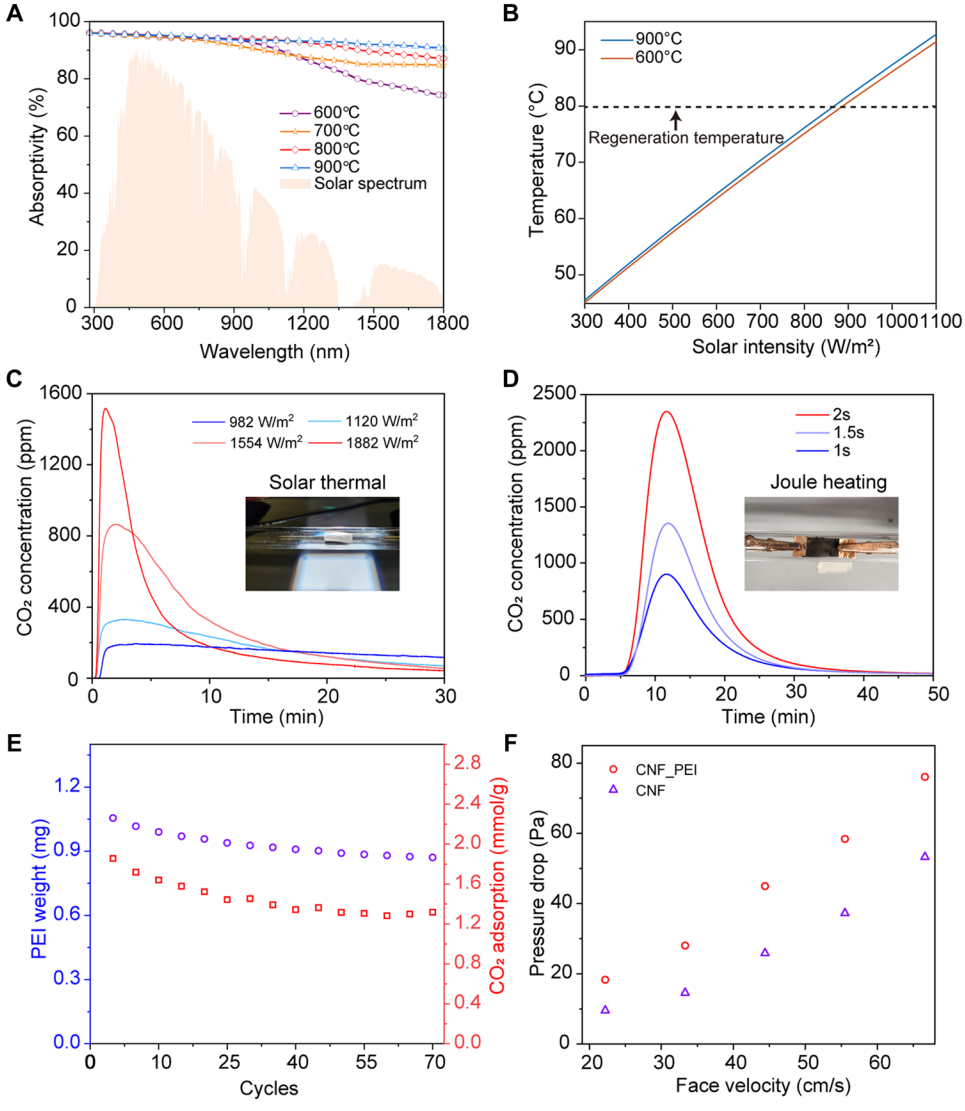

Fig. 3. Regeneration of DAC air filter. (**A**) Solar absorptivity of CNF prepared at different pyrolysis temperatures. (**B**) Simulated temperature of the DAC air filter under different solar intensities. (**C**) Solar regeneration of DAC air filter by solar thermal method at different solar intensities. The inset shows CNF-based adsorbent in a quartz tube under solar light. (**D**) Regeneration of DAC air filter by electrothermal method at different on-site time of 1 s, 1.5 s, and 2 s. (**E**) PEI mass and carbon adsorption capacity of the DAC air filter at different cycle numbers. (**F**) Pressure drop of CNF before and after PEI impregnation.

loading increasing from 16 to 78 wt %, following a similar trend as the adsorption capacity (Fig. 2H).

Another advantage of the CNF-based adsorbent is that CNF is electrically conductive, which enables the CNF framework to be heated up via Joule heating. Compared to the mesoporous silica-based solid DAC adsorbents that can be only regenerated using external thermal sources (*43*, *44*), electrically conductive CNF-based adsorbents are more efficient by localizing the heating near the nanofibers. Moreover, the electrification of the DAC will reduce the total carbon footprint given assess to energy sources, such as hydro, wind, photovoltaic, and geothermal. The sheet resistance of the CNF nonwoven decreased from 16.4 megohms/sq to 38.7 ohms/sq when the pyrolysis temperature was increased from 600° to 900°C (fig. S14) because a more ordered graphite structure was achieved under higher pyrolysis temperatures. The heat capacity of CNF is measured to be only 1.3 J/(g·°C). Together with the nanoscale dimensions and high PEI-to-CNF mass ratio, the sensible heat used to heat the CNF substrate is greatly minimized. In contrast, aqueous solution–based absorbents in the DAC industry, such as the liquid MEA/water system, inevitably require more regeneration energy than PEI-CNF because of the high heat capacity of water [~3.93 J/(g·°C)] (*14*). To demonstrate the electrothermal regeneration capability, PEI-CNF adsorbent is connected to an electric circuit with a digital power supply and solid-state relay (fig. S15). CNF-based adsorbents are connected to the circuit by alligator clips (inset image in Fig. 3D). CO_2 can be effectively released from the adsorbent when a short electrical pulse is applied to the circuit (Fig. 3D).

Temperature-swing cyclability of CNF-based adsorbent is evaluated by in situ thermogravimetric analysis (TGA) via simultaneously switching temperature and N_2/CO_2 atmosphere (fig. S16,

experimental section). CNF-based adsorbent maintains an adsorption capacity of 88.3% after 10 cycles and 72.37% after 40 cycles. After that, the performance became stable, and less capacity drop was noticed. In the next 30 cycles, the performance only drops 0.67% (Fig. 3E). The performance degradation follows a similar trend to the PEI weight loss under cycling thermal regeneration (Fig. 3E), indicating that the performance decrease is primarily due to PEI volatilization or thermal decomposition (*45*, *46*). In addition, the CNF adsorbents have a low pressure drop of 76 Pa at a face velocity of 77 cm/s because the nanofiber dimension is close to the mean free path of air molecules, which allows the air molecules to pass through the fiber smoothly according to the gas slip effect (Fig. 3F) (*47*, *48*). When the face velocity is at a typical HVAC flow rate of 4 m/s, the pressure drop is 392 Pa (fig. S17). The energy consumption required to account for the pressure drop in ventilation and the associated carbon footprint are discussed in Fig. 4.

LCA of CNF-based DAC air filter

The CNF-based adsorbent can be directly integrated downstream of a standard air filter within the building ventilation system, eliminating the requirements of expensive DAC plant constructions. To quantitatively assess the carbon footprint and environmental impact of distributed DAC by the air filters in eliminating 1 kg of CO_2 from direct air, LCA was conducted with the Ecoinvent 3.1 database using OpenLCA software. Figure 4A shows the boundaries of cradle-to-gate and cradle-to-grave (removing and storing 1 kg of CO_2 from direct air) for the DAC air filter system. The cradle-to-gate boundary includes the production and end-of-life treatment of the adsorbent composed of PEI and CNF. The cradle-to-grave boundary covers the cradle-to-gate, DAC operation, and CO_2 storage process. The energy consumption for the DAC operation includes air filter pressure drop, transportation of air filter, regeneration, and vacuum pumping, and the CO_2 storage process includes gas transportation, CO_2 compression, and deep underground injection (text S3).

We first evaluated and compared the cradle-to-gate carbon footprint of different amine-based solid adsorbents, i.e., PEI on alumina, silica, cellulose, and CNF. It is assumed that the mass loadings of PEI on these substrates are each 61%, and the adsorption capacity of the adsorbents is 3 mmol/g based on the experimental results above. The life cycle inventories of PEI and substrates are listed in tables S1 to S6. Figure 4B shows that all four PEI-based adsorbents have a low carbon footprint of 0.039 to 0.055 kg in eliminating 1 kg of CO_2 from direct air. Among them, CNF-based adsorbent has a carbon footprint of 0.049 kg, which is slightly higher than that of alumina and silica-based adsorbents. The cellulose-based adsorbent has the highest carbon footprint of 0.055 kg in the adsorbent life cycle. In addition, compared to the end-of-life treatment of these adsorbents (disposal or recycling), the production of adsorbents accounts for more than 80% of the total carbon emission.

Further, the carbon footprint at various stages of the CCS process—such as transportation, regeneration, pressure drop, vacuum, and CO_2 storage—are assessed in Fig. 4C**.** We compared the carbon emissions when solar thermal and electrothermal technologies were used for adsorbent regeneration. The air filter is assumed to be replaced every 2 days and transported to a centralized processing spot located an average of 10 km from the buildings. For electrothermal regeneration, four types of renewable energy—i.e., hydro, wind, photovoltaic, and geothermal electricity—were chosen for comparison (table S7). DAC air filter with solar thermal regeneration has the lowest carbon emission of 0.073 kg in eliminating 1 kg of CO_2 (table S8). Among them, 67.5% of carbon emissions come from adsorbent production and disposal, while another 24.2% comes from the transportation of adsorbents and CO_2. The regeneration step only accounts for 2.2% of the total carbon emission. This results in a high DAC efficiency of 92.1% in the whole adsorption and operation process. Here, the DAC efficiency for air filter (η_{DAC}) is defined as the ratio of net CO_2 removal to the total captured CO_2 during the cradle-to-gate and operation process

$$\eta_{DAC} = \frac{m_{CO_2,capture} - m_{CO_2,cradle-to-gate\ emission} - m_{CO_2,operation\ emission}}{m_{CO_2,capture}} \times 100\% \quad (1)$$

where $m_{CO_2,capture}$ is the total captured CO_2 by the air filter, and $m_{CO_2,cradle-to-gate\ emission}$, and $m_{CO_2,operation\ emission}$ are the emitted CO_2 from cradle-to-gate and during operation, respectively. Hydroelectricity-powered carbon capture has the lowest carbon footprint of 0.09 kg in eliminating 1 kg of CO_2, followed by wind, photovoltaics, and geothermal, which are 0.15, 0.49, 0.51 kg in eliminating 1 kg of CO_2, respectively (Fig. 4C). The DAC efficiency of these four systems is 90.5, 85.3, 50.5, and 49.4%, respectively (Fig. 4D).

The captured CO_2 can be either stored geologically or used for chemical synthesis (such as fuel synthesis) (*49*), enhanced oil recovery (*50*), food and beverage industry, and the production of coolants and fire retardants (*51*). Over the period 1996 to 2020, 197 million tonnes (Mt) of CO_2 was stored (*52*). Considering the intensified environmental impact and the gigatonne scale of CO_2 removal requirements, geological storage will continue playing a critical role in mitigating CO_2 emissions (*53*). Here, we calculated the carbon footprint and other environmental impacts of carbon capture air filters that with a geological CO_2 storage end stage. It includes CO_2 compressing, transportation to the geological storage site, and injection to the deep sedimentary formation (tables S9 to S12) (*7*, *54*, *55*). The sequestration of 1 kg of CO_2 results in 0.0059 kg of carbon emission when choosing hydropower as energy type (Fig. 4C). Combined with solar thermal technology in adsorbent regeneration, the cradle-to-grave CO_2 removal efficiency ($\eta_{cradle-to-grave}$) of DAC air filter is as high as 92.1% (Fig. 4D). $\eta_{cradle-to-grave}$ is calculated by

$$\eta_{cradle-to-grave} = \eta_{DAC} - \frac{m_{CO_2,storage\ emission}}{m_{CO_2,capture}} \times 100\% \quad (2)$$

where $m_{CO_2,storage\ emission}$ is the carbon footprint during storage. Other environmental impacts such as land use, freshwater ecotoxicity, and human body ecotoxicity for DAC air filters are also evaluated. The land use of air filters using the solar thermal regeneration method is the lowest, followed by hydropower, geothermal, wind, and photovoltaic methods (Fig. 4E). Distributed carbon capture air filters can take advantage of existing ventilation systems, without requirements for additional factory construction, thereby facilitating widespread adoption of carbon capture technologies. In addition, among five regeneration methods, the DAC air filter using solar thermal regeneration shows the lowest freshwater and human body ecotoxicity, further demonstrating its environmental friendliness (Fig. 4F and fig. S18).

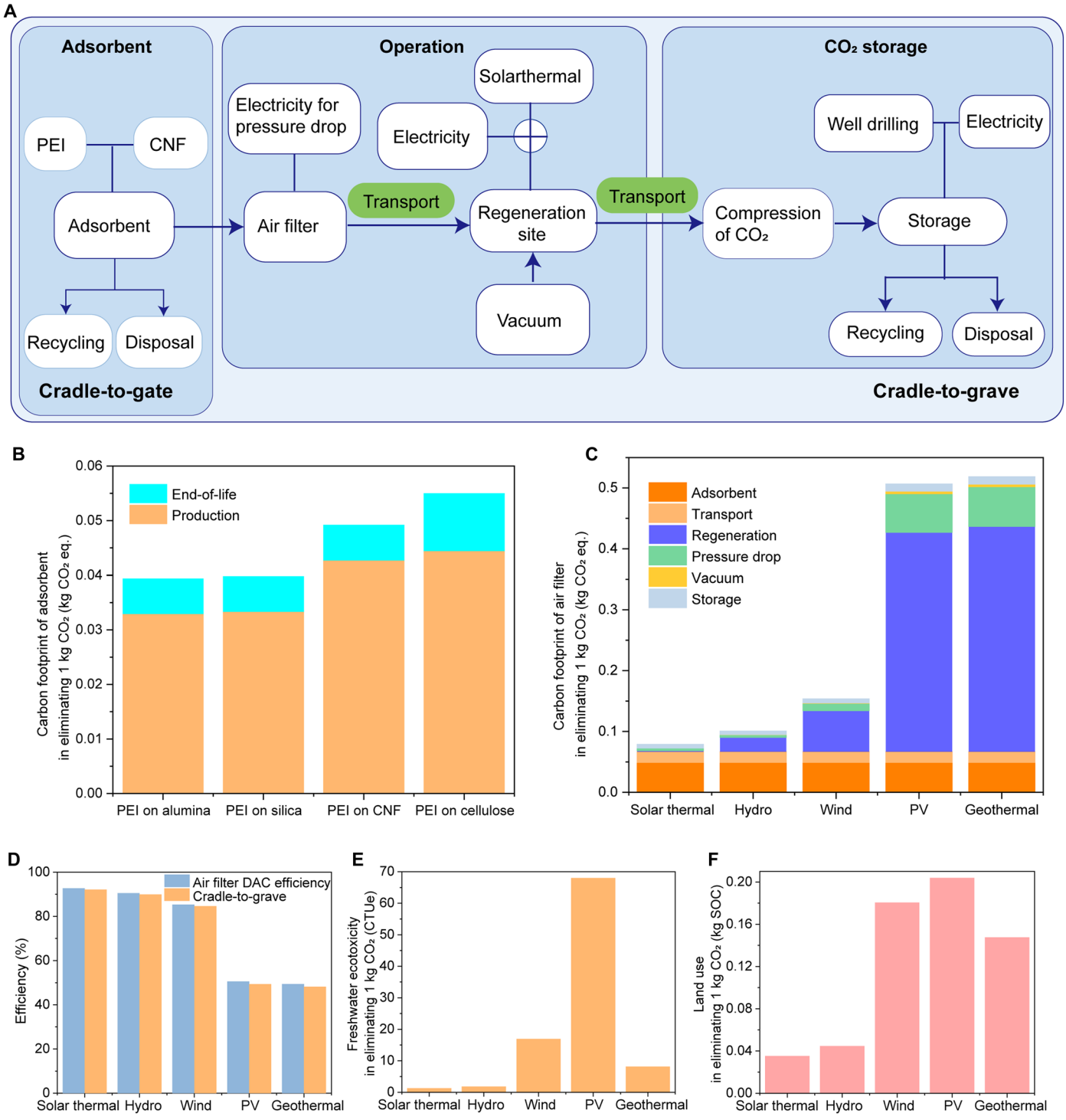

Fig. 4. LCA of distributed DAC and storage process using DAC air filter. (**A**) System boundaries. Cradle-to-gate boundary that including adsorbent production and end-of-life disposal. Cradle-to-grave boundary for DAC air filter, including production, operation, CO_2 storage, and end-of-life disposal. (**B**) Carbon footprint of four different amine-based adsorbents from cradle-to-gate. (**C**) Carbon footprint of DAC and storage process using different electricity supplies from cradle-to-grave. (**D**) Air filter DAC efficiency and cradle-to-grave efficiency in removing CO_2 from direct air. Environmental impacts of (**E**) land use and (**F**) freshwater ecotoxicity for eliminating 1 kg of CO_2 from cradle-to-grave.

TEA of CO_2 capture with CNF-based DAC air filter

To evaluate the economic potential of CNF-based distributed carbon capture, we performed a techno-economic analysis (TEA) for filter production and subsequent CO_2 capture and storage. The TEA was conducted with a discounted cash flow model. First, the levelized cost per filter was estimated for a centralized facility that fabricates 50 million filters per year, which was then used to estimate the cost of CO_2 capture within a city. The number of filters required for a large city of about 10 million people was estimated to capture about 1000 tonne/day of CO_2 (text S4). The filters were assumed to be installed over a 1-year span; thereafter, we assume that 1% of the filters are replaced yearly due to defects and losses. We further estimated the cost associated with filter transportation (from where they are produced and back and forth between CO_2 capture and regeneration sites), the costs of labor, and the cost of CO_2 compression for transportation to the storage site. Please see text S4 for details of economic assumptions and costs.

The cost of DAC using two different regeneration methods, i.e., solar thermal and electrothermal, were assessed, as provided in Fig. 5 (A and B). The estimated total costs are \$362/tonne and \$821/tonne, respectively, with costs being normalized per MT of captured CO_2. When using electrothermal method for regeneration, \$546 is needed to capture 1 tonne of CO_2, which decreases to \$87 when using solar thermal regeneration. In solar thermal scenario, filter production accounts for 64% of the total cost (Fig. 5A). We also estimated the net cost of CO_2 capture and storage by considering the costs associated with CO_2 transportation and underground storage and revenue from CO_2 sales for utilization or 45Q CO_2 capture credits as provided in the Inflation Reduction Act (*56*). This further reduces the total cost of capture and storage or utilization to \$209 to 668/tonne (Fig. 5, C and D, and fig. S19).

DISCUSSION

The advantages of our distributed DAC air filter are fourfold: (i) low capital expenditure for wide CO_2 removal, (ii) improved building sector heating/cooling energy efficiency, (iii) promote public health and productivity, and (iv) efficient and low carbon footprint

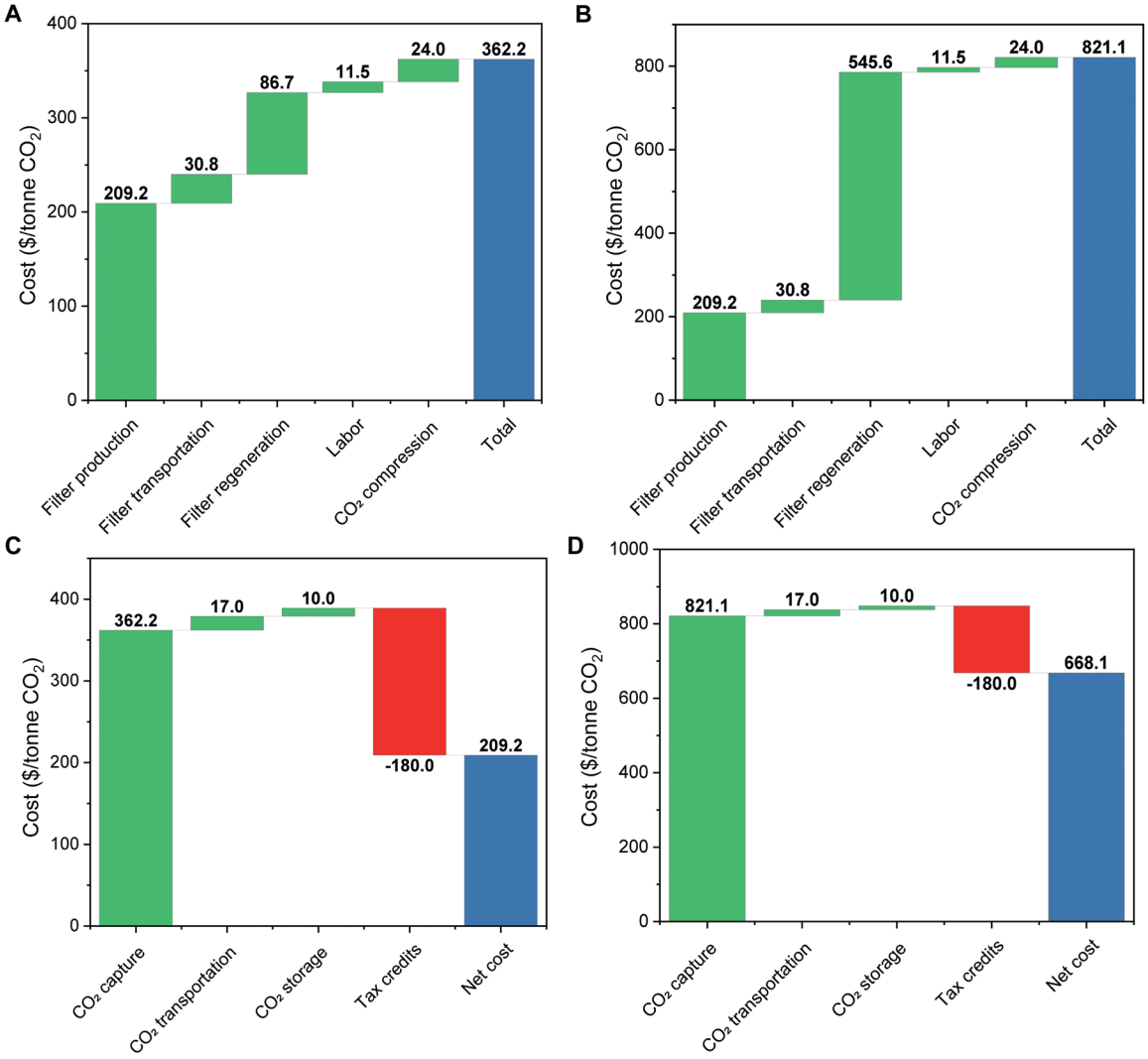

Fig. 5. Levelized cost of distributed CCS by CNF-based air filter. Cost of CO_2 capture using (**A**) solar thermal or (**B**) electrothermal methods for filter regeneration. Levelized cost of CO_2 capture and storage using (**C**) solar thermal method or (**D**) electrothermal methods for filter regeneration.

regeneration. According to the American Society of Heating, Refrigerating, and Air-Conditioning Engineers (ASHRAE) 62.2-2016 standard, the indoor environment is recommended to receive not less than 15 cubic feet per minute per person of outdoor air exchange to ensure indoor air quality and occupant comfort (*57*). For example, cognitive function and productivity decrease when exposed to CO_2 levels above 1000 ppm, with noticeable negative impacts on sleep (*9*, *11*). In addition, the odds of neurophysiologic symptoms such as headache and fatigue largely increase when the CO_2 concentration rises (*58*). If a DAC air filter is retrofitted into the building downstream after conventional air filters, then one can supply CO_2-lean air for the indoor occupants without additional fans/pumps (Fig. 1A). On the basis of the US population distribution in the year 2020, assuming that people spend 90% of their time in indoor environments and that half of the population has access to the air ventilation system that meets the minimal requirements of ASHRAE, the potential CO_2 mitigation amount is calculated to be 25 $MtCO_2\ year^{-1}$ in the United States (Fig. 1B and text S1). Globally, it can potentially further expand to 596 $MtCO_2\ year^{-1}$, which represents about 1.8% of the total annual global CO_2 emissions in 2020. This huge capacity for CO_2 removal could play a crucial role in realizing carbon neutrality. This distributed DAC can be accomplished without high capital expenditure to purchase new land and construct DAC factories, which should facilitate faster deployment and complement well with other DAC technologies.

The distributed DAC benefits the building HVAC energy efficiency by lowering the demand for fresh air intake because of the low indoor CO_2 concentration. As shown in Fig. 1C (a), the conventional ventilation system introduces outside fresh air at the volume flow rate $\dot{V}_1$ to offset the CO_2 generation by occupants and maintain the indoor air quality. Because of the temperature difference between indoor and outdoor environments, the power (P) is needed for heating/cooling this air can be calculated by $P = C_p \rho \dot{V}_1 \Delta T$, where C_p, ρ, and ΔT are the heat capacity, air density, and the indoor/outdoor temperature difference, respectively. Note that we simplify our discussion by focusing on thermal energy rather than the work input of the heat pump or the air conditioner. By adding a carbon capture air filter that can remove the on-site CO_2 in real time [Fig. 1B (b)], the demand for ventilation decreases to $\dot{V}_2 \left(\dot{V}_2 < \dot{V}_1\right)$; therefore, the energy consumption (P_2) also reduces ($P_2 < P_1$). Considering the potential illnesses associated with high (>1000 ppm) indoor CO_2 levels, our DAC air filters can also promote occupants' health and productivity.

After absorbing the CO_2 from direct air, the CNF-based DAC air filters can be regenerated using renewable energy sources, such as sunlight and renewable electricity with high efficiency and extremely low carbon footprint. The desorbed CO_2 can be compressed and sequestrated after separation from water by condensation. The air filter returns to the building for recyclable usage (Fig. 1D). The CNF-based adsorbent can be regenerated under direct sunlight because of its excellent solar absorptivity [Fig. 1E (a)]. Alternatively, it can be regenerated by electrothermal methods using renewable energy resources, such as hydro, wind, photovoltaic, or geothermal [Fig. 1E (b)]. For current industrially mature approaches for DAC regeneration, such as thermal swing adsorption of aqueous KOH solutions (*59*) or amine solutions (*24*–*28*), the adsorbents are heated by external thermal sources, such as boiler or furnace. Because the system's peak temperature must exceed that of the sorbents for effective desorption, substantial energy loss from the heat source to the surroundings is inevitable. Joule heating, on the other hand, provides localized heating directly to the substrate, minimizing the parasitic heat loss. Moreover, because traditional centralized regeneration methods are energy-intensive, choosing a low carbon footprint heat source is crucial to ensure a positive cradle-to-grave carbon capture efficiency, which is why current DAC plants are location sensitive to geothermal or other regeneration energy sources (*54*, *60*). Therefore, to realize distributed DAC, the regeneration energy source must be distributed, which makes renewable electricity and solar thermal the optimal choices.

We conducted LCA to calculate the carbon footprint and carbon removal efficiency of the total CCS process. Solar thermal regeneration gives the highest CO_2 removal efficiency ($\eta_{cradle-to-grave}$), while for air filters regenerated with electrothermal methods, although relative "green" energy types were selected, they still cause immense carbon emissions (Fig. 4C). The underlying reasons for these relatively high carbon footprints originate from the production of energy sources, e.g., 72.5% of carbon emissions in photovoltaic electricity come from the multi-Si wafer photovoltaic panels, and 82.9% of carbon emissions in geothermal electricity come from deep well constructions.

Sensitivity analysis in LCA indicates that the solvent used in adsorbent fabrication largely affects the environmental impacts. When dimethyl sulfoxide is used in PAN electrospinning (*61*), the cradle-to-gate carbon footprint in absorbing 1 kg of CO_2 decreases from 0.049 to 0.044 kg, and the CO_2 removal efficiency increases to 92.6%. In addition, ionization radiation on ecosystem and marine eutrophication decreased by 21.5 and 25.6%, respectively, as shown in table S13. In addition, the carbon footprint is sensitive to the adsorbent cyclability. When the cycling number increases to 4000 times, the CO_2 removal efficiency improves to 95.8% (table S14). Moreover, more PEI mass loading on the CNF support results in a higher carbon capture capacity, enhancing the total CO_2 removal efficiency (table S15).

We conducted TEA to analyze the cost needed in capturing 1 kg of CO_2 from direct air, in comparison to centralized DAC technologies that consist mostly of solid or liquid sorbents. The current costs for centralized DAC range from $100/tonne to more than $1000/tonne (*62*); however, many of the lower range cost estimates rely on waste heat and low-cost electricity. If we assume a low-cost electricity of $30 per megawatt-hour, the levelized cost of CO_2 capture becomes $374/tonne and $541/tonne for solar and electrothermal filter regeneration, respectively (see texts S5 to S7 for more discussion). Compared to DAC, point-source CO_2 capture costs $20 to 200/tonne (*63*), depending on the capture volume and the CO_2 purity in the gas stream. Similarly, there are commercial technologies (e.g., renewable electricity) that prove less expensive in reducing GHG emissions. Our CNF-based adsorbent could also be applied to point-source capture scenarios, where the higher CO_2 partial pressure enhances adsorption capacity. As a result, the cost per metric ton of CO_2 captured would be further reduced. DAC, however, is one of the few processes that addresses the already emitted CO_2, thus potentially enabling negative net greenhouse gas emissions without being dependent on a CO_2 source.

In summary, we demonstrated distributed DAC using the CNF-based air filter to adsorb atmospheric CO_2 in indoor ventilation systems, aiming to exploit the untapped potential for CO_2 removal in urban areas. The DAC air filter not only has the potential to remove 596 $MtCO_2\ year^{-1}$ globally but can also promote building energy efficiency and promote public health and productivity. In addition,

the electrical and optical properties of CNF allow the absorbent to be regenerated at an extremely low carbon footprint, thus increasing the net carbon removal efficiency. The CNF-based adsorbent has a high capacity of 4 mmol/g in a humid atmosphere owing to its porous structure and high PEI mass loading. Regeneration can occur under direct sunlight because of their superior solar absorptivity of 94.4% and low heat capacity of 1.3 J/(g·°C). The CNF has a sheet resistance of 38.7 ohms/sq, enabling it to be electrothermally regenerated using renewable electricity sources. When including the carbon footprint of adsorbent production, operation, CO_2 storage, and disposal, LCA shows that the DAC air filter can achieve a high carbon removal efficiency of 92.1% from cradle-to-grave when using solar thermal technology for regeneration. In addition, TEA results estimate a cost of $209 to $668 for capturing and storing 1 tonne of CO_2 directly from the air. By taking advantage of billions of ventilation systems in the world, distributed DAC air filter technology can shift the paradigm and strengthen the present joint force to confront climate change.

MATERIALS AND METHODS

Preparation of CNF-based DAC air filter

CNF was prepared using electrospinning and pyrolysis of PAN. First, 8 wt % PAN [average molecular weight (M_w) 150,000, (Typical) from Sigma-Aldrich] was dissolved into dimethylformamide by heating at 60°C with stirring for 12 hours until a completely clear solution was obtained. The prepared PAN solution was electrospun under conditions with positive 8-kV voltage at a flow rate of 1 ml/hour. The fibers were collected on a grounded aluminum foil. The distance between the feeding needle (21#) and the collecting electrode was kept at 15 cm. The prepared PAN fibers were dried under vacuum at 60°C overnight to remove the residual solvent. Afterward, PAN nonwoven was oxidized at 260°C for 5 hours in the air. Subsequently, oxidized PAN was transferred to a tube furnace and pyrolyzed at 600° to 900°C under an Ar atmosphere for 2 hours. The ramping rate was set as 5°C/min. To prepare CNF adsorbents with different PEI (branched, average M_w ~800 from Sigma-Aldrich) mass loading, PEI was first dissolved in methanol (high-performance liquid chromatography, from Sigma-Aldrich) at a weight percentage of 1, 2.5, 5, 10, 15, and 20 wt %. After treatment under oxygen plasma (100 W, 5 min), CNF nonwovens were dipped into the PEI/methanol solutions for 5 s and then dried at room temperature to obtain the adsorbents for the DAC air filter.

Absorption isotherms of CNF-based adsorbents

The N_2 and CO_2 adsorption isotherms were measured by 3Flex Micromeritics. For the adsorption isotherms determining the surface area of CNF and adsorbent, the isotherms were measured at 77 K with sample tube merging in the liquid nitrogen. Helium gas was used for free space measurement. The surface area was derived from the N_2 absorption curve using Brunauer-Emmett-Teller theory. The adsorption isotherms for N_2/CO_2 adsorption selectivity were measured at 25°C.

Breakthrough measurements of CNF-based adsorbents

Breakthrough tests were carried out using a homebuilt setup shown in fig. S7. Ar was used as the carrier gas. CO_2 mixture (400 ppm) in N_2 was used for analysis. A mass flow controller (FMA-2617A from Omega Engineering Inc.) was used to control the mass flow rate. KF-16 ring with stainless steel screen for clamp high-vacuum fittings (McMaster-Carr Supply Co.) was used for the sample holder. The sample weight was kept within 1 to 10 mg. A stainless-steel mesh with a size of 0.48 mm^2 was used to fix the sample on the other side before it was connected to the stainless-steel tube. CO_2 concentration was measured using an infrared CO_2 analyzer (Q-S151 from Qubit Systems Inc.). Before breakthrough measurements, the samples were degassed at 120°C for 12 hours in a glove box filled with Ar. The samples were sealed and transferred to the setup with Ar purging through the whole stainless-steel tube until no CO_2 could be detected downstream. For the dry gas breakthrough test, 400 ppm of CO_2/N_2 (used as received) flowed into the sample holder with a flow rate of 8 standard cubic centimeters per minute (sccm). For the wet gas breakthrough test, the 400 ppm of CO_2/N_2 gas was first purged through a water reservoir, and then the mixture of gas with water molecules was purged through the sample holder. The humidity of the mixture gas was controlled by the water level in the sink, and it was measured using a humidity sensor (SEK-SHT31-Sensors). For the capacity measurements at different humid conditions (fig. S6), the flow rate is 20 sccm. Analytical grade CO_2, N_2, Ar, and He from Airgas Inc. were used as received.

Regeneration of CNF-based adsorbents

CNF-based adsorbents were regenerated using the breakthrough setup equipped with a quartz tube as the sample holder. For solar-driven regeneration, a solar simulator was used to simulate the sunlight with different powers. For joule heating regeneration, CNF-based adsorbent was connected to two copper alligator clips, which were further connected to a power supply and a solid-state relay. A functional generator was used to control the switching time for the electric circuit.

Cyclability measurements of CNF-based adsorbents

The CO_2 capture cyclic performance was investigated by a thermogravimetric analyzer (TGA, TA Instruments Q50). A sample flow of 60 ml/min and a balance flow of 40 ml/min were used for the analysis. A sample weight of ~5 mg was used for measurement. Before the cyclic test, the sample was first heated to 105°C in an N_2 environment to remove the adsorbed CO_2 and H_2O. One adsorption-desorption cycle includes two steps. For absorption, the temperature was decreased to 25°C, and CO_2 gas was purged to the adsorbents through the sample flow at 200 ml/min. For desorption, the temperature was increased to 105°C in the N_2 atmosphere. The CO_2 adsorption time was 2 hours. The temperature ramping rate was set as 10°C/min.

Optical characterizations of CNF-based adsorbents

The ultraviolet (UV)–visible–near-infrared absorption (A) spectra were derived after measuring transmission (T) and reflection (R) spectra ($A = 1 - R - T$) by Shimadzu UV-3600 spectrophotometer equipped with a barium sulfate integration sphere (ISR-1503). The incident angle was set as 0°. A barium sulfate standard white plate was used for baseline measurements. FTIR spectra were measured by Shimadzu IRTracer-100 FTIR spectrophotometer with Gladi-ATR (diamond prism) single-bounce ATR mode.

Other characterizations

The SEM images and EDS of the CNF nonwoven were taken by a high-resolution field emission scanning electron microscope

(Carl Zeiss Merlin). TEM images were taken on FEI Tecnai G2 F30 300 kV Super Twin Electron Microscope. XPS and XRD spectra were taken using the Kratos AXIS Nova and Rigaku SmartLab, respectively. Raman spectrum was measured by HORIBA LabRAM HR Evolution Confocal Raman Microscope. Pressure drop is measured by a differential pressure gauge (EM201B, UEi Test Instruments). Sheet resistance was measured by a Signatone Pro4 probe stand with an SP4 probe head and a Keysight B2901A precision source/measure unit. The heat capacity was measured by the TA Instruments Discovery 2500 differential scanning calorimeter.

Supplementary Materials

This PDF file includes:

Supplementary Text S1 to S7
Figs. S1 to S22
Tables S1 to S19
References

REFERENCES AND NOTES

1. H. Wang, J. Liu, M. Klaar, A. Chen, L. Gudmundsson, J. Holden, Anthropogenic climate change has influenced global river flow seasonality. *Science* **383**, 1009–1014 (2024).
2. A. Momeni, R. V. McQuillan, M. S. Alivand, A. Zavabeti, G. W. Stevens, K. A. Mumford, Direct air capture of CO_2 using green amino acid salts. *Chem. Eng. J.* **480**, 147934 (2024).
3. Z. Liu, Z. Deng, S. Davis, P. Ciais, Monitoring global carbon emissions in 2022. *Nat. Rev. Earth Environ.* **4**, 205–206 (2023).
4. K. S. Lackner, S. Brennan, J. M. Matter, A.-H. A. Park, A. Wright, B. Van Der Zwaan, The urgency of the development of CO_2 capture from ambient air. *Proc. Natl. Acad. Sci. U.S.A.* **109**, 13156–13162 (2012).
5. E. S. Sanz-Pérez, C. R. Murdock, S. A. Didas, C. W. Jones, Direct capture of CO_2 from ambient air. *Chem. Rev.* **116**, 11840–11876 (2016).
6. J. K. Soeherman, A. J. Jones, P. J. Dauenhauer, Overcoming the entropy penalty of direct air capture for efficient gigatonne removal of carbon dioxide. *ACS Eng. Au* **3**, 114–127 (2023).
7. E. National Academies of Sciences, and Medicine, *Negative Emissions Technologies and Reliable Sequestration: A Research Agenda* (National Academies Press, 2019).
8. M. Ozkan, S. P. Nayak, A. D. Ruiz, W. Jiang, Current status and pillars of direct air capture technologies. *iScience* **25**, 103990 (2022).
9. T. A. Jacobson, J. S. Kler, M. T. Hernke, R. K. Braun, K. C. Meyer, W. E. Funk, Direct human health risks of increased atmospheric carbon dioxide. *Nat. Sustain.* **2**, 691–701 (2019).
10. M. Benammar, A. Abdaoui, S. H. Ahmad, F. Touati, A. Kadri, A modular IoT platform for real-time indoor air quality monitoring. *Sensors* **18**, 581 (2018).
11. M. Kang, Y. Yan, C. Guo, Y. Liu, X. Fan, P. Wargocki, L. Lan, Ventilation causing an average CO_2 concentration of 1,000 ppm negatively affects sleep: A field-lab study on healthy young people. *Build. Environ.* **249**, 111118 (2024).
12. C. Sui, J. Pu, T.-H. Chen, J. Liang, Y.-T. Lai, Y. Rao, R. Wu, Y. Han, K. Wang, X. Li, V. Viswanathan, P.-C. Hsu, Dynamic electrochromism for all-season radiative thermoregulation. *Nat. Sustain.* **6**, 428–437 (2023).
13. Y. Dong, M. Coleman, S. A. Miller, Greenhouse gas emissions from air conditioning and refrigeration service expansion in developing countries. *Annu. Rev. Env. Resour.* **46**, 59–83 (2021).
14. N. El Hadri, D. V. Quang, E. L. V. Goetheer, M. R. M. Abu Zahra, Aqueous amine solution characterization for post-combustion CO_2 capture process. *Appl. Energy* **185**, 1433–1449 (2017).
15. S. Zhou, X. Chen, T. Nguyen, A. K. Voice, G. T. Rochelle, Aqueous ethylenediamine for CO_2 capture. *ChemSusChem* **3**, 913–918 (2010).
16. H. Seo, T. A. Hatton, Electrochemical direct air capture of CO_2 using neutral red as reversible redox-active material. *Nat. Commun.* **14**, 313 (2023).
17. A. Hemmatifar, J. S. Kang, N. Ozbek, K. J. Tan, T. A. Hatton, Electrochemically mediated direct CO_2 capture by a stackable bipolar cell. *ChemSusChem* **15**, e202102533 (2022).
18. J. H. Rheinhardt, P. Singh, P. Tarakeshwar, D. A. Buttry, Electrochemical capture and release of carbon dioxide. *ACS Energy Lett.* **2**, 454–461 (2017).
19. R. Sharifian, R. Wagterveld, I. Digdaya, C. Xiang, D. Vermaas, Electrochemical carbon dioxide capture to close the carbon cycle. *Energ. Environ. Sci.* **14**, 781–814 (2021).
20. P. Zhu, Z.-Y. Wu, A. Elgazzar, C. Dong, T.-U. Wi, F.-Y. Chen, Y. Xia, Y. Feng, M. Shakouri, J. Y. Kim, Continuous carbon capture in an electrochemical solid-electrolyte reactor. *Nature* **618**, 959–966 (2023).
21. J. C. Abanades, Y. A. Criado, H. I. White, Direct capture of carbon dioxide from the atmosphere using bricks of calcium hydroxide. *Cell Rep. Phys. Sci.* **4**, 101339 (2023).
22. Z. Li, X. Guo, X. Xue, X. Xu, B. Wang, Investigations on kinetics and mechanisms of $CaCO_3$ calcination in calcium looping. *Ind. Eng. Chem. Res.* **62**, 4851–4863 (2023).
23. J. Blamey, E. Anthony, J. Wang, P. Fennell, The calcium looping cycle for large-scale CO_2 capture. *Prog. Energy Combust. Sci.* **36**, 260–279 (2010).
24. H. Mao, J. Tang, G. S. Day, Y. Peng, H. Wang, X. Xiao, Y. Yang, Y. Jiang, S. Chen, D. M. Halat, A scalable solid-state nanoporous network with atomic-level interaction design for carbon dioxide capture. *Sci. Adv.* **8**, eabo6849 (2022).
25. G. Zainab, A. A. Babar, N. Iqbal, X. Wang, J. Yu, B. Ding, Amine-impregnated porous nanofiber membranes for CO_2 capture. *Compos. Commun.* **10**, 45–51 (2018).
26. G. N. Short, E. Burentugs, L. Proaño, H. J. Moon, G. Rim, I. Nezam, A. Korde, S. Nair, C. W. Jones, Single-walled zeolitic nanotubes: advantaged supports for poly(ethylenimine) in CO_2 separation from simulated air and flue gas. *JACS Au* **3**, 62–69 (2023).
27. Y. Labreche, R. P. Lively, F. Rezaei, G. Chen, C. W. Jones, W. J. Koros, Post-spinning infusion of poly(ethyleneimine) into polymer/silica hollow fiber sorbents for carbon dioxide capture. *Chem. Eng. J.* **221**, 166–175 (2013).
28. A. Goeppert, M. Czaun, R. B. May, G. S. Prakash, G. A. Olah, S. Narayanan, Carbon dioxide capture from the air using a polyamine based regenerable solid adsorbent. *J. Am. Chem. Soc.* **133**, 20164–20167 (2011).
29. H. A. Evans, D. Mullangi, Z. Deng, Y. Wang, S. B. Peh, F. Wei, J. Wang, C. M. Brown, D. Zhao, P. Canepa, Aluminum formate, $Al(HCOO)_3$: An earth-abundant, scalable, and highly selective material for CO_2 capture. *Sci. Adv.* **8**, eade1473 (2022).
30. S. He, B. Zhu, X. Jiang, G. Han, S. Li, C. H. Lau, Y. Wu, Y. Zhang, L. Shao, Symbiosis-inspired de novo synthesis of ultrahigh MOF growth mixed matrix membranes for sustainable carbon capture. *Proc. Natl. Acad. Sci. U.S.A.* **119**, e2114964119 (2022).
31. M. Fasihi, O. Efimova, C. Breyer, Techno-economic assessment of CO_2 direct air capture plants. *J. Clean. Prod.* **224**, 957–980 (2019).
32. D. V. Quang, A. V. Rabindran, N. El Hadri, M. R. Abu-Zahra, Reduction in the regeneration energy of CO_2 capture process by impregnating amine solvent onto precipitated silica. *Eur. Sci. J.* **9**, 82–102 (2013).
33. D. T. Nguyen, R. Truong, R. Lee, S. A. Goetz, A. P. Esser-Kahn, Photothermal release of CO_2 from capture solutions using nanoparticles. *Energ. Environ. Sci.* **7**, 2603–2607 (2014).
34. P. Li, T.-J. Zhao, J.-H. Zhou, Z.-J. Sui, Y.-C. Dai, W.-K. Yuan, Characterization of carbon nanofiber composites synthesized by shaping process. *Carbon* **43**, 2701–2710 (2005).
35. X. Shen, H. Du, R. H. Mullins, R. R. Kommalapati, Polyethylenimine applications in carbon dioxide capture and separation: From theoretical study to experimental work. *Energ. Technol.* **5**, 822–833 (2017).
36. R. B. Said, J. M. Kolle, K. Essalah, B. Tangour, A. Sayari, A unified approach to CO_2–amine reaction mechanisms. *ACS Omega* **5**, 26125–26133 (2020).
37. J. Yu, S. S. Chuang, The structure of adsorbed species on immobilized amines in CO_2 capture: An in situ IR study. *Energy Fuel* **30**, 7579–7587 (2016).
38. U. Tumuluri, M. Isenberg, C.-S. Tan, S. S. Chuang, In situ infrared study of the effect of amine density on the nature of adsorbed CO_2 on amine-functionalized solid sorbents. *Langmuir* **30**, 7405–7413 (2014).
39. W. Zhang, H. Liu, Y. Sun, J. Cakstins, C. Sun, C. E. Snape, Parametric study on the regeneration heat requirement of an amine-based solid adsorbent process for post-combustion carbon capture. *Appl. Energy* **168**, 394–405 (2016).
40. N. Iqbal, X. Wang, J. Yu, B. Ding, Robust and flexible carbon nanofibers doped with amine functionalized carbon nanotubes for efficient CO_2 capture. *Adv. Sustain. Syst.* **1**, 1600028 (2017).
41. M. Al-Marri, M. Khader, M. Tawfik, G. Qi, E. Giannelis, CO_2 sorption kinetics of scaled-up polyethylenimine-functionalized mesoporous silica sorbent. *Langmuir* **31**, 3569–3576 (2015).
42. W. Sagues, H. Jameel, D. Sanchez, S. Park, Prospects for bioenergy with carbon capture & storage (BECCS) in the United States pulp and paper industry. *Energ. Environ. Sci.* **13**, 2243–2261 (2020).
43. F. Rezaei, R. P. Lively, Y. Labreche, G. Chen, Y. Fan, W. J. Koros, C. W. Jones, Aminosilane-grafted polymer/silica hollow fiber adsorbents for CO_2 capture from flue gas. *ACS Appl. Mater. Interfaces* **5**, 3921–3931 (2013).
44. D. V. Quang, A. Dindi, M. R. Abu-Zahra, One-step process using CO_2 for the preparation of amino-functionalized mesoporous silica for CO_2 capture application. *ACS Sustain. Chem. Eng.* **5**, 3170–3178 (2017).
45. H. V. Thakkar, A. J. Ruba, J. A. Matteson, M. P. Dugas, R. P. Singh, Accelerated testing of PEI-silica sorbent pellets for direct air capture. *ACS Omega* **9**, 45970–45982 (2024).
46. G. Qi, Y. Wang, L. Estevez, X. Duan, N. Anako, A.-H. A. Park, W. Li, C. W. Jones, E. P. Giannelis, High efficiency nanocomposite sorbents for CO_2 capture based on amine-functionalized mesoporous capsules. *Energ. Environ. Sci.* **4**, 444–452 (2011).
47. Y. Bian, L. Zhang, C. Chen, Experimental and modeling study of pressure drop across electrospun nanofiber air filters. *Build. Environ.* **142**, 244–251 (2018).

48. X. Zhao, S. Wang, X. Yin, J. Yu, B. Ding, Slip-effect functional air filter for efficient purification of PM2. 5. *Sci. Rep.* **6**, 35472 (2016).
49. R. Schäppi, D. Rutz, F. Dähler, A. Muroyama, P. Haueter, J. Lilliestam, A. Patt, P. Furler, A. Steinfeld, Drop-in fuels from sunlight and air. *Nature* **601**, 63–68 (2022).
50. M. L. Godec, V. A. Kuuskraa, P. Dipietro, Opportunities for using anthropogenic CO_2 for enhanced oil recovery and CO2 storage. *Energy Fuel* **27**, 4183–4189 (2013).
51. Q. Zhu, Developments on CO_2-utilization technologies. *Clean Energy* **3**, 85–100 (2019).
52. Y. Zhang, C. Jackson, S. Krevor, An estimate of the amount of geological CO_2 storage over the period of 1996–2020. *Environ. Sci. Technol. Lett.* **9**, 693–698 (2022).
53. S. Krevor, H. de Coninck, S. E. Gasda, N. S. Ghaleigh, V. de Gooyert, H. Hajibeygi, R. Juanes, J. Neufeld, J. J. Roberts, F. Swennenhuis, Subsurface carbon dioxide and hydrogen storage for a sustainable energy future. *Nat. Rev. Earth Environ.* **4**, 102–118 (2023).
54. S. Deutz, A. Bardow, Life-cycle assessment of an industrial direct air capture process based on temperature–Vacuum swing adsorption. *Nat. Energy* **6**, 203–213 (2021).
55. T. Terlouw, K. Treyer, C. Bauer, M. Mazzotti, Life cycle assessment of direct air carbon capture and storage with low-carbon energy sources. *Environ. Sci. Technol.* **55**, 11397–11411 (2021).
56. J. A. Yarmuth, H.R.5376 - 117th Congress (2021-2022): Inflation Reduction Act of 2022 (2022); www.congress.gov/bill/117th-congress/house-bill/5376.
57. Standard 62. 2–2013 Ventilation for Acceptable Indoor Air Quality (ANSI/ASHRAE, 2013); https://ierga.com/wp-content/uploads/sites/2/2017/10/ASHRAE-62.2-2013.pdf.
58. N. Muscatiello, A. McCarthy, C. Kielb, W. H. Hsu, S. A. Hwang, S. Lin, Classroom conditions and CO_2 concentrations and teacher health symptom reporting in 10 New York State Schools. *Indoor Air* **25**, 157–167 (2015).
59. D. W. Keith, G. Holmes, D. S. Angelo, K. Heidel, A process for capturing CO_2 from the atmosphere. *Joule* **2**, 1573–1594 (2018).
60. H. Li, M. E. Zick, T. Trisukhon, M. Signorile, X. Liu, H. Eastmond, S. Sharma, T. L. Spreng, J. Taylor, J. W. Gittins, Capturing carbon dioxide from air with charged-sorbents. *Nature* **630**, 654–659 (2024).
61. L. Sabantina, M. Klöcker, M. Wortmann, J. R. Mirasol, T. Cordero, E. Moritzer, K. Finsterbusch, A. Ehrmann, Stabilization of polyacrylonitrile nanofiber mats obtained by needleless electrospinning using dimethyl sulfoxide as solvent. *J. Ind. Text* **50**, 224–239 (2020).
62. R. Chauvy, L. Dubois, Life cycle and techno-economic assessments of direct air capture processes: An integrated review. *Int. J. Energy Res.* **46**, 10320–10344 (2022).
63. G. Zang, P. Sun, E. Yoo, A. Elgowainy, A. Bafana, U. Lee, M. Wang, S. Supekar, Synthetic methanol/Fischer–Tropsch fuel production capacity, cost, and carbon intensity utilizing CO_2 from industrial and power plants in the United States. *Environ. Sci. Technol.* **55**, 7595–7604 (2021).
64. A. Sinha, L. A. Darunte, C. W. Jones, M. J. Realff, Y. Kawajiri, Systems design and economic analysis of direct air capture of CO_2 through temperature vacuum swing adsorption using MIL-101(Cr)-PEI-800 and mmen-Mg2(dobpdc) MOF adsorbents. *Ind. Eng. Chem. Res.* **56**, 750–764 (2017).
65. "National assessment of geologic carbon dioxide storage resources: summary," (2013); https://pubs.usgs.gov/publication/fs20133020.
66. U.S. Energy Information Administration, "Form EIA-861M, Monthly Electric Power Industry Report" (2025); www.eia.gov/electricity/monthly/epm_table_grapher.php?t=epmt_5_6_a.
67. U.S. Energy Information Administration, "Short-Term Energy Outlook" (2025); www.eia.gov/outlooks/steo/.
68. E. Smith, J. Morris, H. Kheshgi, G. Teletzke, H. Herzog, S. Paltsev, The cost of CO_2 transport and storage in global integrated assessment modeling. *Int. J. Greenh. Gas Control* **109**, 103367 (2021).
69. S. Hughes, A. Zoelle, M. Woods, S. Henry, S. Homsy, S. Pidaparti, N. Kuehn, H. Hoffman, K. Forrest, A. Sheriff, T. Fout, W. Summers, S. Herron, "Cost of capturing CO2 from industrial sources" (DOE/NETL-2022/3319, National Energy Technology Laboratory, 2022); https://doi.org/10.2172/1887586.
70. A. Damodaran, Cost of equity and capital (US) (Damodaran Online, 2025); https://pages.stern.nyu.edu/~adamodar/New_Home_Page/datafile/wacc.html.
71. Federal reserve bank of St. Louis, 10-year breakeven inflation rate (2025); https://fred.stlouisfed.org/series/T10YIE.
72. A. Pujol, M. Heuckendorff, T. Helmer Pedersen, Techno-economic analysis of two novel direct air capture-to-urea concepts based on process intensification. *J. Clean. Prod.* **496**, 144932 (2025).
73. A. von Harpe, H. Petersen, Y. Li, T. Kissel, Characterization of commercially available and synthesized polyethylenimines for gene delivery. *J. Control. Release* **69**, 309–322 (2000).
74. G. W. Meijer, G. Kanny, J. F. Briois, *Ullmann's encyclopedia of industrial chemistry* (Wiley, 2000).
75. S. Weber, J. F. Peters, M. Baumann, M. Weil, Life cycle assessment of a vanadium redox flow battery. *Environ. Sci. Technol.* **52**, 10864–10873 (2018).
76. A. Roes, L. Tabak, L. Shen, E. Nieuwlaar, M. Patel, Influence of using nanoobjects as filler on functionality-based energy use of nanocomposites. *J. Nanopart. Res.* **12**, 2011–2028 (2010).
77. R. Husgafvel, K. Vanhatalo, L. Rodriguez-Chiang, L. Linkosalmi, O. Dahl, Comparative global warming potential assessment of eight microcrystalline cellulose manufacturing systems. *J. Clean. Prod.* **126**, 620–629 (2016).
78. M. P. Mahmud, N. Huda, S. H. Farjana, C. Lang, Environmental impacts of solar-photovoltaic and solar-thermal systems with life-cycle assessment. *Energies* **11**, 2346 (2018).
79. Volpe National Transportation Systems Center, "National Transportation Statistics 2021 [50th Anniversary Edition]" (Bureau of Transportation Statistics, 2021); https://doi.org/10.21949/1523389.
80. V. Núñez-López, E. Moskal, Potential of CO_2-EOR for near-term decarbonization. *Front. Clim.* **1**, 5 (2019).

Acknowledgments: We thank P. Griffin for the help in setting the TGA and 3Flex Micromeritics. We thank P. Julson and J. Robles for the help in building the breakthrough measurement setup. We thank W. Chen for the discussion about LCA. This work made use of the shared facilities at the University of Chicago Materials Research Science and Engineering Center. Parts of this work were carried out at the Soft Matter Characterization Facility of the University of Chicago. **Funding:** This work was supported by the Startup Fund by Pritzker School of Molecular Engineering, University of Chicago (to P.-C.H.); the ACS Petroleum Research Fund (PRF) 67770-ND10 (to P.-C.H.); and the National Science Foundation under award numbers DMR-2011854 and DMR- 2114117 (to D.B.M.). **Author contributions:** P.-C.H. and R.W. conceived the idea. R.W. performed the sample preparation, characterizations, and corresponding data analysis. H.E.D. and A.E. conducted the TEA and guided the LCA calculations. Y.X., D.B.M., G.M.H., and A.R. helped with the TGA measurement and analysis. G.Y. and Y.H. helped with SEM characterization. E.L. helped with electrospinning. Q.L. helped with the CO_2 analyzer setup. Y.C. helped with regeneration measurements. Q. F. helped with the TEM characterization. A.S. helped with isotherm measurements. P.-C.H. and C.L. guided the air filter design. P.-C.H. supervised the whole project. R.W. and P.-C.H. wrote the manuscript with input from all co-authors. **Competing interests:** The authors declare that they have no competing interests. **Data and materials availability:** All data needed to evaluate the conclusions in the paper are present in the paper and/or the Supplementary Materials.

Submitted 7 January 2025
Accepted 19 September 2025
Published 17 October 2025
10.1126/sciadv.adv6846

ScienceAdvances

Distributed direct air capture by carbon nanofiber air filters

Ronghui Wu, Hernan E. Delgado, Yi Xie, Yuanke Chen, Gangbin Yan, Edward Luo, Qizhang Li, Qingsong Fan, Yu Han, Genesis M. Higueros, Amar Ruthen, Chenxi Sui, Adarsh Suresh, David B. Mitzi, Chong Liu, Amgad Elgowainy, and Po-Chun Hsu

Sci. Adv. **11** (42), eadv6846. DOI: 10.1126/sciadv.adv6846

Science Advances (ISSN 2375-2548) is published by the American Association for the Advancement of Science. 1200 New York Avenue NW, Washington, DC 20005. The title *Science Advances* is a registered trademark of AAAS.